Molecular Catalysis xxx (2017) xxx–xxx

Contents lists available at ScienceDirect

Molecular Catalysis

journal homepage: www.elsevier.com/locate/mcat

Kinetic and mechanistic study of triose sugar conversion on Lewis and Brønsted acid solids

E.A. Pighin, J.I. Di Cosimo, V.K. Díez*

Catalysis Science and Engineering Research Group (GICIC), INCAPE, UNL-CONICET, CCT CONICET Santa Fe, Colectora Ruta Nac. 168, km 0, Paraje "El Pozo", (3000) Santa Fe, Argentina

ARTICLE INFO

Article history:
Received 10 August 2017
Received in revised form 11 October 2017
Accepted 21 November 2017
Available online xxx

Keywords:
Dihydroxyacetone
Ethyl lactate
Lewis and Brønsted solid acid catalysts
Kinetic modeling

ABSTRACT

The effect of catalyst acid site nature on the reaction kinetics of the liquid-phase conversion of dihydroxyacetone with ethanol was investigated using Brønsted and Lewis acid solids. The reaction proceeds through a complex reaction network involving a sequence of consecutive and parallel reaction steps. Main final products were ethyl lactate and pyruvic aldehyde diethyl acetal. Different catalysts such as the cesium salt of tungstophosphoric acid (Cs-HPA), Amberlyst resin and alumina-supported tin and zinc oxides were used. Catalysts were characterized by ICP, X-ray diffraction, N_2 physisorption, TPD of NH_3 and FTIR of adsorbed pyridine. Cs-HPA contains only Brønsted acid sites and alumina-supported tin and zinc samples show exclusively Lewis acidity. During dihydroxyacetone conversion, the selectivities to the final products strongly depend on the nature of the surface acid sites present on the solids. Brønsted acid solids favor the synthesis of pyruvic aldehyde diethyl acetal with final yields of up to 93%, whereas the ethyl lactate is the main product on Lewis acid solids, reaching final yields of about 51%. A kinetic model based on a pseudohomogeneous mechanism was proposed to interpret the experimental catalytic data. The comparison of the kinetic rate constants obtained on both kinds of acid solids confirms that on Brønsted catalysts the route toward pyruvic aldehyde diethyl acetal is clearly favored. On Lewis solids, the synthesis of ethyl lactate occurs selectively via isomerization of the pyruvic aldehyde hemiacetal intermediate.

1. Introduction

There is an increasing worldwide interest in deriving chemicals from biomass. Materials containing cellulose and starch are attractive candidates for its transformation in more valuable compounds. These resources can be converted in sugars in biorefineries; sugars in turn are molecules that can give rise to a number of chemicals and liquid fuels [1,2]. In fact, sugars resulting from cellulose enzymatic hydrolysis [1,3], can be converted by fermentation in many platform compounds for the production of valuable C3-C6 derivatives. Particularly, glucose can be transformed by retroaldol reactions in short carbon chain polyfunctional compounds containing C=O and OH groups. Thus, dihydroxyacetone (DHA), a monosaccharide that belongs to the group of trioses, can be obtained from glucose and subsequently transformed in more valuable oxygenates such as ethyl lactate (EL) and pyruvic aldehyde diethyl acetal (PADA), Scheme 1.

Alkyl lactates are biodegradable nontoxic compounds with high boiling points; these properties make them excellent green solvents. They are used as plasticizer [4] and in surfactant and in herbicide formulations. Also, they are employed in the cosmetic industry as skin whitener and in acne treatments [5]. In particular, EL is used as green solvent, plasticizer, and in pharmaceutical and cosmetic formulations. On the other hand, PADA is employed as intermediate in the synthesis of folic acid [6] and of an osteoporosis inhibitor [7].

In the last years, many works describe the reactions between triose sugars and short chain alcohols using solid acid catalysts. The literature reports the use of zeolites [8–11], mixed oxides [12] and substituted mesoporous materials such as Al and Ga/MCM-41 [13] as catalysts. More recently, it has been postulated the use of Sn-containing catalysts such as mesoporous materials (Sn-MCM-41 [13,14], Sn-SBA-15 [15], Sn-Si mixed oxides [16]), clays like montmorillonite [17] and zeolites (Sn-MFI [18], Sn-BEA [19–23]) which showed to be highly active and selective toward alkyl lactates. However, the use of mesoporous and zeolitic materials during the conversion of DHA presents several draw backs such as the costly and time demanding synthesis procedures. Given this, in a previ-

* Corresponding author.
E-mail address: verodiez@fiq.unl.edu.ar (V.K. Díez).

http://dx.doi.org/10.1016/j.mcat.2017.11.026
2468-8231/

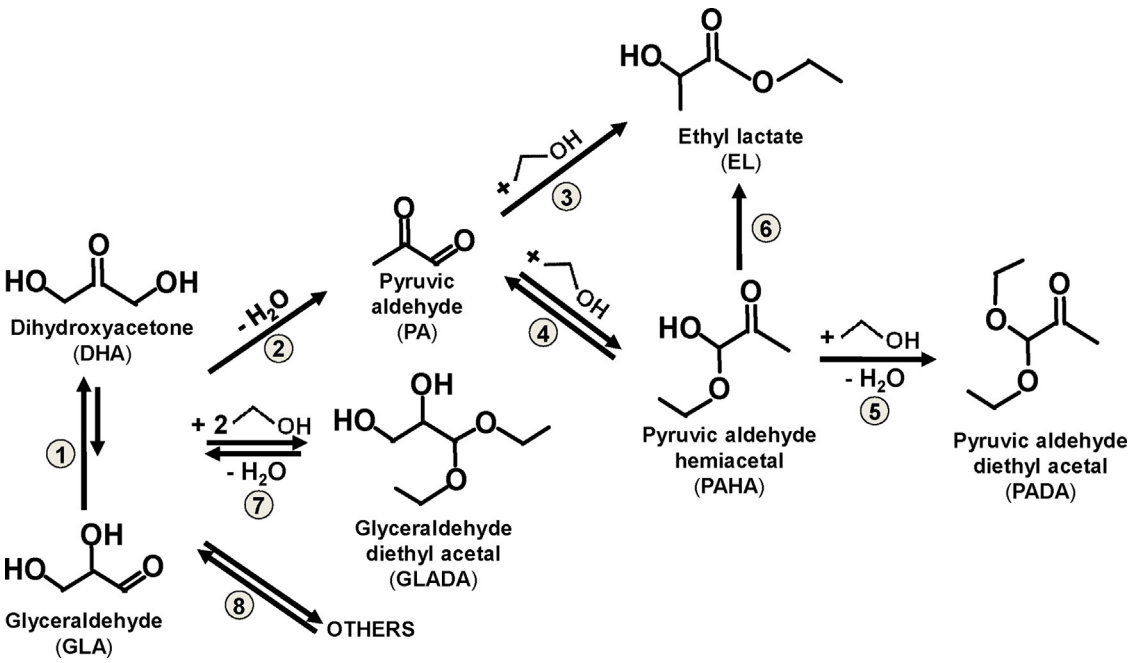

Scheme 1. Reaction pathways for the conversion of C_3 monosaccharides via dehydration, ethanol nucleophilic addition and esterification reactions on solid catalysts with Lewis and Brønsted acid properties [25].

ous work [24] we investigated the conversion of DHA and ethanol on inexpensive alumina-supported Sn catalysts obtained by incipient wetness impregnation. We showed that on these Lewis acid materials high ethyl lactate yields (≈70%) are obtained at mild conditions. We focused there on the role of the surface Sn species in the generation of more and stronger Lewis acid sites than those present on the alumina support. Also, we demonstrated that the ethyl lactate yield is enhanced as the Sn loading increases, confirming the participation of these sites in rate-limiting steps. Although the DHA conversion reaction has been extensively studied in our and other previous works, very few efforts have been made so far to determine the kinetics and the mechanistic features of the different reaction steps involved in the reaction pathway of Scheme 1.

Given this, we have focused on the kinetic study of the DHA conversion reactions on Lewis acid solids (Sn/Al_2O_3 catalysts) [25]; we analyzed the effect of Sn loading and reaction temperature on the ethyl lactate yield and on the reaction kinetics and postulated a pseudohomogeneous mechanism that gave a suitable description of the complex reaction system (Scheme 1). We found that the kinetic parameter associated to ethyl lactate formation increases with the number of Lewis acid sites confirming that surface Sn species are responsible for the catalytic activity of these materials.

However, there was still a lack in the literature of kinetic studies of DHA conversion investigating comparatively solid catalysts with Brønsted and Lewis acidity. This is why, in this work, we continue our investigations on the reaction kinetics involved in the DHA conversion but comparing the catalytic performance of solids with Brønsted (cesium salt of tungstophosphoric acid and Amberlyst 35W resin) and Lewis (Sn/Al_2O_3, and Zn/Al_2O_3) acid properties. Our goal was to elucidate the effect of the catalyst acid nature on determining the selectivity toward the final product, EL or PADA. Furthermore, we performed a kinetic study of the reaction system by modeling experimental data using a pseudohomogeneous model. We focused on the competitive pathways leading to PADA and EL presented in Scheme 1 and identified the steps of the reaction network promoted by Lewis or Brønsted sites.

2. Experimental

2.1. Catalyst synthesis and activation

Alumina-supported tin and zinc oxides were prepared by incipient wetness impregnation of commercial γ-Al_2O_3 Cyanamid Ketjen CK 300. Aqueous solutions of $SnCl_4{\cdot}5H_2O$ (Aldrich, 98%) and $Zn(NO_3)_2$ (Aldrich, 98%) were used; samples were coded as SnAl and ZnAl, respectively. The SnAl and ZnAl precursors were thermally decomposed overnight (18 h) in flowing air at 573 K. The chemical content of Sn and Zn in both alumina-supported metal oxides was around 7.0 wt.%.

ZnO was obtained by decomposition of commercial $(ZnCO_3)_2(Zn(OH)_2)_3$ (Anedra) in air at 623 K. On the other hand, SnO_2 was prepared by precipitation of a solution of $SnCl_4{\cdot}5H_2O$ (Aldrich, 98%) with aqueous solution of urea (Anedra, 99%). The precipitate was then decomposed in air at 573 K overnight in order to obtain the corresponding pure tin oxide. More details are given elsewhere [26].

The cesium salt of the tungstophosphoric acid ($Cs_{2.5}H_{0.5}PW_{12}O_{40}$), coded as Cs-HPA, was prepared by slowly adding an aqueous solution of Cs_2CO_3 (Sigma-Aldrich, PA 99.9%) to an aqueous solution of $H_3PW_{12}O_{40}$, HPA (Merck, PA). The precipitate was heated overnight at 353 K and then calcined in N_2 flow at 573 K.

A commercial Amberlyst 35W resin (Rohm and Haas) was used; pellets were crushed and sieved to retain particles between 180 and 480 μm. The resulting powder was treated in a N_2 flow at 373 K before the catalytic test.

2.2. Catalyst characterization

BET surface areas (*SA*) were measured by N_2 physisorption at 77 K using an Autosorb Quantachrome 1-C sorptometer. The catalyst Sn or Zn chemical content was analyzed by inductively coupled plasma (ICP-OES). The sample structural properties were analyzed by X-Ray Diffraction (XRD) technique using a Shimadzu XD-D1

Please cite this article in press as: E.A. Pighin, et al., Kinetic and mechanistic study of triose sugar conversion on Lewis and Brønsted acid solids, Mol. Catal. (2017), http://dx.doi.org/10.1016/j.mcat.2017.11.026

instrument with nickel filtered Cu Kα radiations between 10 and 80°.

Total acid site numbers (n_a) were measured by TPD of NH_3. Samples were thermally treated in He at the corresponding calcination temperature and then exposed to a 1.01% NH_3/He flow at 373 K during 30 min in order to reach surface saturation. Weakly adsorbed NH_3 was removed by flushing with He. The temperature was then increased from 373 K to 973 K for Cs-HPA and Al_2O_3 samples, using a ramp rate of 10 K/min. In the case of SnAl and ZnAl, the temperature was increased up to 593 K and then kept constant at this temperature for 1 h. NH_3 concentration in the reactor effluent was monitored using a mass spectrometer (MS) detector.

Identification of the chemical nature of the acid sites present on the catalyst surface was carried out by Infrared Spectroscopy (IR) of pyridine adsorbed at room temperature and evacuated at increasing temperatures. Experiments were performed with a Shimadzu FTIR Prestige-21 spectrophotometer. An inverted T-shaped cell containing the sample wafer and fitted with CaF_2 windows was used. In a typical experiment, the sample wafer was evacuated at 573 K and then cooled down to room temperature to take the catalyst spectrum. After that, the sample was exposed to 0.12 kPa of pyridine at room temperature and then evacuated consecutively at 298, 373, 423, 473 and 573 K. The resulting spectrum at each evacuation temperature was recorded at room temperature. Spectra of the adsorbed species were obtained by subtracting the catalyst spectrum. In all the spectra, the absorbance scales were normalized to 20-mg wafers.

2.3. Catalytic testing

Liquid-phase conversion of dihydroxyacetone, DHA (Aldrich, 97%) and ethanol (Merck, 99.8%) was carried out at 353 K and at an autogenous pressure of 250 KPa in a batch PARR reactor. A solution of DHA in ethanol with DHA/ethanol = 0.023 (molar ratio) was loaded in the reactor. The catalyst/DHA weight ratio was 43%. Catalysts were thermally treated ex-situ in air at the corresponding calcination temperature to remove adsorbed water. After introducing the reactant mixture, the reactor was sealed and flushed with N_2 and then the mixture was heated up to the reaction temperature under stirring (400 rpm). Then, the catalyst as ground powder was added to the reaction mixture to start the reaction. Inter- and intra-particle diffusional limitations were verified to be negligible. For this purpose, the Mears number [27] was calculated to evaluate the extent of the external mass transfer resistance. On the other hand, the Weisz-Prater criterion [28] for a first order reaction and spherical catalyst particles was used to verify the absence of intra-particle mass transfer limitations. More details are given elsewhere [25]. During the experiments, 13 samples of ≈0.5 mL were extracted from the reactor. Product identification was achieved using a Thermo Scientific Trace 1300 GC with a Thermo Scientific TR-5MS capillary column coupled to a Thermo Scientific ISQ QD MS unit. Product analysis and quantification were done using a 7890A Agilent Technologies GC equipped with a FID detector and a Carbowax Amine 30 M capillary column. The concentration, C_j, of the main reaction products (pyruvic aldehyde (PA), ethyl lactate (EL), pyruvic aldehyde hemiacetal (PAHA), pyruvic aldehyde diethyl acetal (PADA) and glyceraldehyde diethyl acetal (GLADA)) was calculated by this technique. For quantification purposes, *n*-octanol was used as external standard.

Product yields (Y_j, mole of product *j*/mole of DHA fed) were calculated as $Y_j = S_j\, X_{DHA}$ where X_{DHA} is the dihydroxyacetone conversion ($X_{DHA} = (n^0{}_{DHA} - n_{DHA})/n^0{}_{DHA}$, where $n^0{}_{DHA}$ are the moles of dihydroxyacetone initially loaded and n_{DHA} are the moles of dihydroxyacetone at the reaction time *t*) and S_j is the selectivity of product *j* (S_j, mole of product *j*/mole of DHA reacted). Selectivities were calculated as $S_j = C_j/\Sigma C_j$, where C_j is the concentration of product *j*.

The initial DHA conversion rate (r^0_{DHA}, mmol/h g_{cat}) was calculated from the initial slope of the X_{DHA} vs. $tW/n^0{}_{DHA}$ (corrected time) curve, where *W* is the catalyst weight.

2.4. Kinetic modeling and statistical analysis

A kinetic study was carried out by modeling the catalytic data using a first-order pseudohomogeneous model. More details will be given in *Section* 3.3.

The system of differential equations was solved numerically using the Microsoft Excel Solver software and the Euler method. This calculation tool uses the Generalized Reduced Gradient (GRG) algorithm for optimizing non-linear problems.

The experimental relative molar concentrations of all the species during the reaction (C^*_{jobs}) were compared with the values predicted by the model (C^*_{jcalc}). The kinetic parameters (k_i) of each reaction step of Scheme 1 were estimated by minimizing the sum of the squared errors (*SSE*) [29] between the experimental and model data as:

$$SSE = \sum_{\substack{alldata \\ samples}} \left(C^*_{jcalc} - C^*_{jobs}\right)^2 \quad (1)$$

where C^0_{DHA} is the initial DHA concentration in the reactor expressed in mmol DHA/cm^3. The relative concentration of compound *j* $\left(C^*_j\right)$ is defined as C_j/C^0_{DHA}. The coefficient of determination (R^2) gives the fitting quality [29] and was calculated using Eq. (2):

$$R^2 = \frac{\sum_{i=1}^{n}\left(C^*_{jcalc} - \bar{C}^*_{jobs}\right)^2}{\sum_{i=1}^{n}\left(C^*_{jobs} - \bar{C}^*_{jobs}\right)^2} \quad (2)$$

where $\bar{C}^*_{jobs}$ is the mean of measured values.

The discrimination between models was carried out using the model selection criterion (*MSC*) [30], according to Eq. (3):

$$MSC = \ln\left[\frac{\Sigma\left(C^*_{Jobs} - \bar{C}^*_{Jobs}\right)^2}{\Sigma\left(C^*_{Jobs} - C^*_{Jcalc}\right)^2}\right] - \frac{2p}{m} \quad (3)$$

where *p* is the number of parameters; *m* is the number of experimental observations. The *MSC* parameter is used to compare statistically different models so that the larger the *MSC* value, the better the fit and the more appropriate the model for interpreting the data.

3. Results and discussion

3.1. Catalyst characterization

The solid acid catalysts prepared by different methods and commercial Amberlyst resin were characterized; their chemical, structural, textural and acid properties were investigated. Results are summarized in Table 1, where properties of the γ-Al_2O_3 support are included as reference. Catalyst metal contents (Zn and Sn) were around 7.0 wt.%. Through the different procedures used for preparing the catalysts, solids withsurface area (*SA*) values higher than 140m^2/g were obtained. The SnAl and ZnAl samples presented lower surface areas than the γ-Al_2O_3 support, probably due to a partial pore blockage by metal species during the impregnation procedure. On the other hand, the substitution of the protons of the bulk HPA structure by Cs^+ cations promotes a 16-fold increase

Please cite this article in press as: E.A. Pighin, et al., Kinetic and mechanistic study of triose sugar conversion on Lewis and Brønsted acid solids, Mol. Catal. (2017), http://dx.doi.org/10.1016/j.mcat.2017.11.026

Table 1
Chemical, textural and acidic properties of solid catalysts.

Catalyst	Surface area, SA (m^2/g)	Metal loading[a] (wt.%)	Surface acidic properties			
			Acid site number, n_a [b] (μmol/g)	Acid site nature [d]		
				L/(L+B) (%)	Lewis band position (cm^{-1})	
					ν 19b	ν 8a
SnAl	184	6.9	165	100.0	1453	1617
ZnAl	183	6.6	59	99.2	1450	1613
Cs-HPA	143	–	47	0.0	–	–
Amberlyst 35W	52	–	5200[c]	*nd*	*nd*	*nd*
γ-Al_2O_3	230	–	24	99.1	1450	1616

B: Brønsted sites, L: Lewis sites; *nd*: not determined.
[a] by ICP.
[b] by TPD of NH_3.
[c] data provided by the supplier.
[d] by FTIR of pyridine desorbed at 423 K.

of *SA* value (SA_{HPA} = 9 m^2/g), which is in agreement with a previous report [31]. In addition to the significant higher *SA*, bulk Cs-HPA was employed instead HPA because the former is insoluble in the alcoholic medium of the reaction, in contrast to the known solubility of bulk tungstophosphoric acid in oxygen-containing polar solvents [32,33].

The structural properties of ZnAl and SnAl catalysts and pure Al_2O_3, SnO_2 and ZnO oxides were analyzed by XRD. The XRD patterns of tin and zinc alumina-supported oxides (see Fig. S1 in *Supplementary Material*) exhibit broad signals corresponding to quasi-amorphous γ-Al_2O_3. No crystalline tin phases were observed on SnAl sample thereby indicating that Sn species are well dispersed on the alumina surface forming small SnO_2 domains not detectable by XRD. Furthermore, the XRD pattern of the ZnAl sample shows a barely perceptible ZnO phase indicating a probably lower dispersion of the ZnO species on alumina. On the other hand, the structure of Cs-HPA was confirmed by XRD analysis (Fig. S1) and also the XRD pattern obtained for this sample was consistent with those reported previously in the literature [34].

The surface acid properties of SnAl, ZnAl and Cs-HPA samples were investigated by combining TPD of NH_3 preadsorbed at 373 K and FTIR of pyridine adsorbed at room temperature. Characterization of Amberlyst 35W resin by these techniques was not possible due to the low thermal stability of this sample. The NH_3 TPD profile of Cs-HPA (see Fig. S2 in *Supplementary Material*) showed several desorption peaks at temperatures in the range of 450–850 K, reflecting the presence on this sample of surface acid species that bind NH_3 with different strength. Furthermore, Cs-HPA is the sample with the strongest acid sites, with NH_3 still desorbing at temperatures higher than 815 K. On the other hand, the NH_3 TPD profiles of SnAl and ZnAl (Fig. S2) exhibit a broad asymmetric desorption peak around 580–600 K.

For the analyzed catalysts, the total amount of NH_3 desorbed from the surface was measured by integration of the TPD curves and it was taken as an indication of the total acid site number, n_a (μmol/g). The n_a values are reported in Table 1. Sample SnAl exhibits the highest n_a value. In fact, the addition of tin species to the Al_2O_3 support produces almost a 7-fold increase of n_a whereas the incorporation of zinc on Al_2O_3 generates a much lower increase of n_a (2.5 times, Table 1). This result is in line with the lower dispersion of the ZnO species compared to those of SnO_2 observed by XRD. Later, the differences in acidic properties between SnAl and ZnAl catalysts will be further discussed.

The identification of the chemical nature of the surface acid sites of SnAl, ZnAl, Al_2O_3 and Cs-HPA samples was performed by analyzing the FTIR spectra of adsorbed pyridine after admission at 298 K and sequential evacuation at increasing temperatures; the spectra

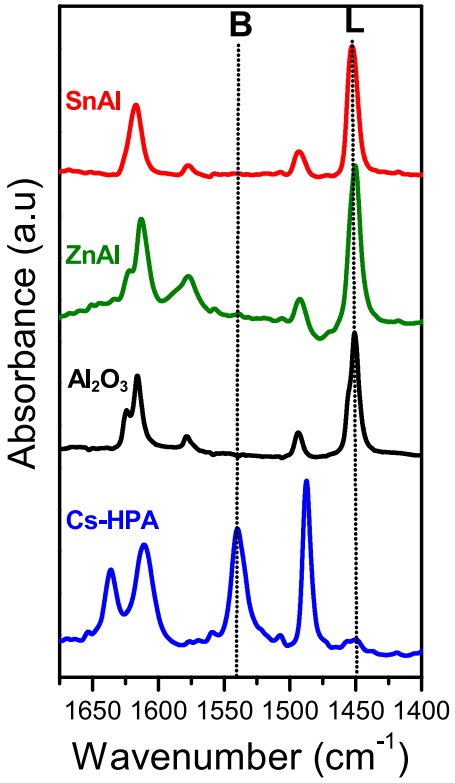

Fig. 1. FTIR of pyridine adsorbed at room temperature and evacuated at 423 K on Lewis and Brønsted acid catalysts.

after evacuation at 423 K are shown in Fig. 1. Cs-HPA showed the typical bands of pyridinium ion formed by protonation of pyridine on Brønsted acid sites. These bands are the ring vibrations modes at 1636, 1608, 1537 and 1485 cm^{-1} [35]. On the other hand, only the bands at 1622, 1615 and 1455 cm^{-1}, assigned to pyridine coordinated on the oxide cations, were detected in the spectra of the SnAl and ZnAl samples. Thus, SnAl and ZnAl contain Lewis acid centers [36]. This was confirmed by calculating the relative contribution of the Brønsted (B) and Lewis (L) acid sites, L/(L+B), by integration of the bands at ~1540 and ~1450 cm^{-1}, respectively, Table 1. Results show that Lewis acid centers represent about 99–100% of the total acid site number of samples SnAl and ZnAl, whereas Cs-HPA does not exhibit Lewis acidity. On the other hand, commercial Amberlyst 35W, which could not be characterized, is a solid with well-known Brønsted acidic properties confirmed in a previous work [37].

Please cite this article in press as: E.A. Pighin, et al., Kinetic and mechanistic study of triose sugar conversion on Lewis and Brønsted acid solids, Mol. Catal. (2017), http://dx.doi.org/10.1016/j.mcat.2017.11.026

Moreover, an analysis of the strength of the Lewis acid sites was performed for the SnAl, ZnAl and Al_2O_3 samples based on the position of the adsorbed pyridine bands at around 1450 cm^{-1} and 1620 cm^{-1}, that correspond to ν19b and ν8a vibration modes, respectively, Fig. 1. On SnAl these bands shift to higher frequencies compared with ZnAl (Table 1), thereby suggesting stronger acid sites on the former [38].

3.2. Effect of the acid site nature on catalytic performance during DHA conversion

The effect of the chemical nature (Brønsted or Lewis) of the catalyst surface acid sites during the conversion of dihydroxyacetone (DHA) was investigated. The catalytic performance of different Brønsted and Lewis acid solids was evaluated under identical reaction conditions. These conditions were selected based on previous experiments and literature where mixed oxides, zeolites and mesoporous materials were used in this reaction [12–14,23,24,25]. Pure Al_2O_3 was also tested for comparative purposes.

In previous work [25], we postulated the reaction pathway for triose conversion depicted in Scheme 1. Dihydroxyacetone and glyceraldehyde (GLA), (step 1) are easily interconvertible and lead to similar product distribution [8]. Therefore, they are equally suitable as substrates for the synthesis of ethyl lactate (EL) and pyruvic aldehyde diethyl acetal (PADA). Thus, global conversion of trioses during catalytic experiments, X_{DHA}, involves, in fact, the conversion of DHA and GLA. The following step is the triose dehydration to pyruvic aldehyde, PA (step 2 in Scheme 1). From PA the reaction pathway might proceed toward EL by re-arrangement with incorporation of an alcohol molecule (step 3), or toward pyruvic aldehyde diethyl acetal, PAHA (step 4) and PADA (step 5) by addition of an alcohol molecule in each of these reaction steps. Step 6 is the isomerization of PAHA to EL.

Table 2 summarizes the catalytic results obtained with all the acid solids investigated. The alumina support resulted poorly active under our reaction conditions in spite of being a Lewis acid solid (Fig. 1). Thus, it seems that the Al^{3+} cations are not acidic enough to transform DHA.

Different activities (r^0_{DHA} values in Table 1) were obtained depending on the Brønsted or Lewis acid properties of the different solid materials. However, as will be discussed later, the nature of the acidity is not the only factor determining activity.

Main products obtained from triose conversion were the intermediate products PA and PAHA, and the terminal products EL and PADA (Scheme 1). As can be seen in Table 2, on the catalysts with high r^0_{DHA} values (SnAl, Cs-HPA and Amberlyst 35W), the final yields (Y_j) toward EL and PADA, are strongly dependent on the acid nature of the active sites.

Brønsted solids favored the synthesis of PADA over that of EL; on Cs-HPA and Amberlyst 35W, both with strong Brønsted acid properties, PADA was the major product. In particular, yields of PADA of 93% were reached at the end of the 7 h run on Amberlyst resin. However, at higher conversion levels Cs-HPA resulted less active and selective than Amberlyst, giving other undesirable products. The selective formation of PADA on these solids is not a matter of conversion level since the EL/PADA ratio calculated at low conversions (Table 2) for all the catalysts showed similar trend.

The performance of Lewis acid solids during triose conversion was investigated in detail in previous works [24,25]. We prepared and characterized similar SnAl catalysts and studied the effect of varying the tin loading (between 1.4–7.6 wt.%), tin precursor ($SnCl_2$ or $SnCl_4$) and reaction temperature (between 353 and 373 K) on the activity and product distribution. We demonstrated that the SnAl catalysts produce selectively EL and that the catalytic performance of these materials can be improved by increasing Sn content to 7.6 wt.% [24] and the reaction temperature to 373 K [25], to reach a final Y_{EL} value of 70%. Here, the SnAl catalyst with 6.9 wt.% Sn reached complete DHA conversion at 7 h of reaction at 353 K, giving a moderate final Y_{EL} of 51% and minor amounts of the other products.

Our catalytic results obtained on Lewis and Brønsted acid solids (Table 2) are in line with previous works reported in the literature. Pescarmona et al. [8] and Clippel et al. [14] found that zeolites with high concentration of strong Brønsted sites catalyze the formation of the diacetal product, in agreement with the findings of Table 2 for Cs-HPA and Amberlyst 35W. On the other hand, zeolites combining mild Brønsted acidity with Lewis acidity arising from extra-framework aluminum species, promote the formation of alkyl lactates with yields between 54 and 59% [8].

Regarding Lewis acid properties, the effect of changing the Lewis metal cation of the alumina-supported catalysts was also investigated by preparing and characterizing Sn- and Zn-promoted materials. Zeolites and mesoporous materials containing structural Sn species have been widely reported in the literature for converting trioses into alkyl lactates [13,14,19]. That was the input to select Sn as a Lewis acid cation. However, Sn in the SnAl catalyst reported here has a different chemical environment compared to zeolites or MCM-41 materials. We also selected Zn as a promoter of Lewis acidity based on the fact that several authors claimed that ZnBEA [39] and zincosilicates are strong Lewis acids [40,41] and therefore they are attractive catalytic materials for the conversion of sugars, in particular, for the Lewis acid- or Brønsted/Lewis acid-catalyzed isomerization of glucose to fructose [41].

The two Lewis acid solids investigated here (SnAl and ZnAl) exhibit values of EL/PADA ratio (Table 2) between 2.2 and 3.0, confirming that on these samples EL is the main reaction product at low conversions. However, the ZnAl sample was considerably less active to convert DHA than SnAl, showing an initial DHA conversion rate value ≈10 times lower. Similarly, on ZnAl the final X_{DHA} and Y_{EL} values were clearly lower than those of SnAl.

The characterization results of the Lewis acid samples (Table 1) show an important effect of the Sn promotion on the enhanced acidic properties (number and strength of the acid sites) of SnAl compared to Al_2O_3. That can be explained considering that the catalyst Lewis acidity is related to the oxide electronegativity (χ_{oxide}). According to Sanderson, the electronegativity of an oxide with the formula M_yO_x, is: $\chi_{oxide} = [(\chi_M)^y(\chi_O)^x]^{1/(y+x)}$ [42]. Time ago, we calculated χ_{oxide} for a series of M_yO_x single oxides and showed an acceptable correlation between χ_{oxide} and n_a, in spite of the former being a bulk property [43]. The χ_{oxide} calculated for Al_2O_3 (2.53) was similar to that of ZnO (2.38) and lower than that of SnO_2 (2.85). Thus, more acidic SnO_2 forming highly dispersed surface Sn species is responsible for the noticeable increase of the surface acidic properties of the SnAl sample compared to the support (Table 1). On the contrary, surface promotion of Al_2O_3 with the less acidic zinc oxide produces only a slight increase of the acid site number (Table 1), thereby explaining the poor catalytic performance of this catalyst.

In addition to the lower acidity of ZnO compared to SnO_2, the marked difference between the catalytic performance of SnAl and ZnAl samples could be attributed to the different way in which Sn and Zn species interact with the support during impregnation and subsequent calcination procedures. Bulkier ZnO oxide species were generated on the ZnAl sample, as indicated by the XRD data, suggesting a lower affinity of the Zn^{2+} cations for the alumina surface.

Furthermore, Hayashi and Sasaki [44] reported the homogeneously-catalyzed conversion of trioses with alcohols. Working with different alcoholic solutions of metal chlorides (MCl_n) they found that most of the chlorides, such as $ZnCl_2$, were inactive for the reaction and only tin chlorides ($SnCl_n$) were able to produce high yields of alkyl lactates. They attributed the distinct performance of the $SnCl_n$ salts to their ability to strongly coordi-

Please cite this article in press as: E.A. Pighin, et al., Kinetic and mechanistic study of triose sugar conversion on Lewis and Brønsted acid solids, Mol. Catal. (2017), http://dx.doi.org/10.1016/j.mcat.2017.11.026

Table 2
Results obtained during DHA conversion on different acid solid catalysts.

Catalyst	Initial DHA conversion rate, r^0_{DHA} (mmol/hg)	EL/PADA selectivity ratio[a]	Catalytic results at t = 7 h					
			DHA conversion, X_{DHA} (%)	Product yields, Y_j (%)				
				PA	PAHA	EL	PADA	GLADA
SnAl	30.4	3.0	98.6	15.7	0.2	50.9	11.1	16.0
ZnAl	3.6	2.2	19.8	2.2	2.5	1.6	0.7	2.8
Cs-HPA	26.4	0.2	70.9	3.3	4.6	0.3	41.9	0.2
Amberlyst 35W	54.3	0.1	98.8	0.3	0.4	3.5	93.1	0.2
Al_2O_3	2.5	–	11.0	1.3	6.7	3.1	0.0	0.0

Reaction conditions: T = 353 K, DHA/ethanol (molar) = 0.023, W_{cat}/W_{DHA} = 43 wt.%.
[a] at X_{DHA} ≈10–20%.

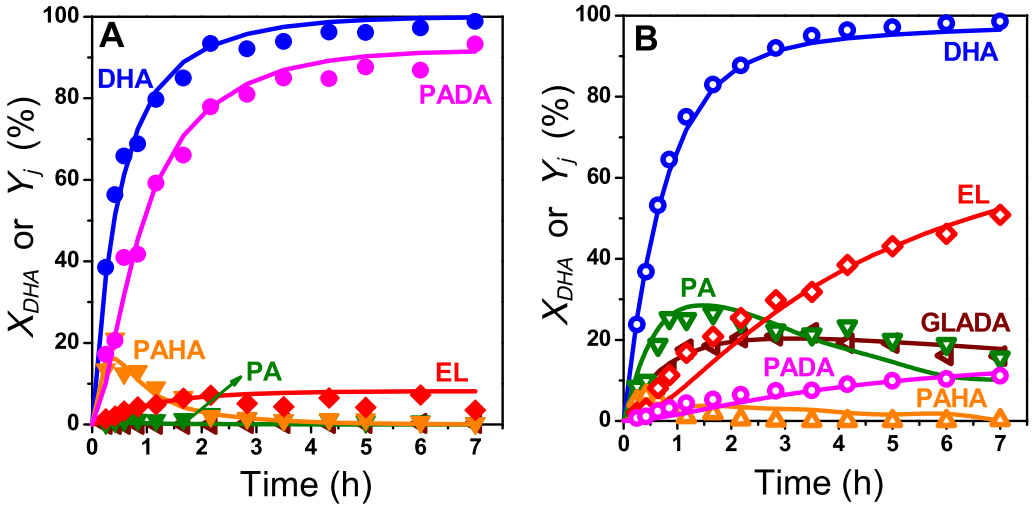

Fig. 2. DHA conversion (X_{DHA}) and product yields (Y_j) vs reaction time on Amberlyst 35W (A) and SnAl (B). [T = 353 K, DHA/ethanol (molar) = 0.023, W_{cat}/W_{DHA} = 43 wt.%]. Points, experimental results; solid lines, model predictions.

nate to PA to form a specific intermediate in which a 1,2-hydride shift occurs to predominantly yield the alkyl lactate.

It seems then that whereas Zn-based materials promote the isomerization of sugars, they are not able to promote the complex reaction pathway involved in the ethyl lactate synthesis.

3.3. Reaction kinetic modeling and surface mechanisms

Fig. 2 shows the catalytic tests on Amberlyst 35W and SnAl, representing typical Brønsted and Lewis acid solids, respectively. In agreement with the reaction pathways postulated in Scheme 1, the shape of product yield vs time curves of Fig. 2, shows that PA and PAHA are intermediate compounds. On the other hand, the zero initial slopes of the EL and PADA yield curves and the fact that these curves do not exhibit maxima, suggests they are secondary and terminal products of the reaction. According to these results and as mentioned in Section 3.2, the conversion of DHA with ethanol seems to proceed by an initial dehydration step and further rearrangement into PA. PA is then converted into the EL or PAHA via ethanol addition; the latter can undergo consecutive esterification to PADA. Similar reaction pathways were proposed previously in the literature [8,9,14].

In an attempt to analyze comparatively the performance of our Lewis and Brønsted catalysts and to gain insight into the reaction mechanism, a kinetic study was carried out by modeling the catalytic data of Fig. 2 using a pseudohomogeneous model. One of the purposes of the kinetic modeling was to identify which of the reaction steps of the reaction network (Scheme 1) is promoted by Lewis or Brønsted acid sites.

The kinetic modeling of the experimental data obtained during DHA conversion on Brønsted and Lewis acid solids was carried out considering different assumptions for the pseudohomogeneous model. The only products of triose (DHA and GLA) conversion were PA, EL, PAHA, PADA, GLADA; unidentified products present in low concentration in the reaction mixture were grouped as OTHERS. First order kinetics respect to the DHA and products were considered; taking into account that the concentration of ethanol is in excess respect to the stoichiometric concentration, the initial ethanol concentration (C^0_{EtOH}) remains constant during the typical 7-h run and therefore, the reaction order for ethanol was taken as zero.

Initially, we followed here a strategy consisting of considering all the steps of Scheme 1 as reversible reactions, but small values of the kinetic constants for the reverse reactions of steps 2, 3, 5 and 6 were obtained. Then, we repeated the calculations assuming that these were irreversible steps whereas steps 4, 7 and 8, were considered as reversible transformations. Finally, in an attempt to elucidate which of the two possible pathways toward EL, either the direct synthesis from PA (step 3) or the isomerization of PAHA (step 6), was kinetically favored under our reaction conditions, we carried out two more calculations of the kinetic parameters assuming in one case that $k_6 = 0$ and that $k_3 = 0$ in the other. We compared the kinetic and statistical parameters in both cases and we found that the best results were obtained considering that on both catalysts the synthesis of EL occurs exclusively from PAHA via isomerization reaction. Thus, the highest value of the coefficient of determination (R^2) and the lowest value of the sum of the squared errors (*SSE*) were obtained when the kinetic constant of the direct synthesis of EL from PA was considered equal to zero ($k_3 = 0$).

Please cite this article in press as: E.A. Pighin, et al., Kinetic and mechanistic study of triose sugar conversion on Lewis and Brønsted acid solids, Mol. Catal. (2017), http://dx.doi.org/10.1016/j.mcat.2017.11.026

The mass balances for the different components of reaction mixture, are given by the differential Eqs. (4)–(10):

$$\frac{n^0_{DHA}}{W}\frac{dC^*_{DHA}}{dt} = -r_2 - r_7 - r_8 \quad (4)$$

$$\frac{n^0_{DHA}}{W}\frac{dC^*_{PA}}{dt} = r_2 - r_4 \quad (5)$$

$$\frac{n^0_{DHA}}{W}\frac{dC^*_{EL}}{dt} = r_6 \quad (6)$$

$$\frac{n^0_{DHA}}{W}\frac{dC^*_{PAHA}}{dt} = r_4 - r_5 - r_6 \quad (7)$$

$$\frac{n^0_{DHA}}{W}\frac{dC^*_{PADA}}{dt} = r_5 \quad (8)$$

$$\frac{n^0_{DHA}}{W}\frac{dC^*_{GLADA}}{dt} = r_7 \quad (9)$$

$$\frac{n^0_{DHA}}{W}\frac{dC^*_{OTHERS}}{dt} = r_8 \quad (10)$$

where C^*_j is the relative concentration of compound j (C_j/C^0_{DHA}); r_2, r_4, r_5, r_6, r_7 and r_8 are the reaction rates of step 2, 4, 5, 6, 7 and 8, respectively, in Scheme 1, expressed in mmol/hg.

On the other hand, the mathematics equations for the proposed model are given in Eqs. (11)–(16) before re-parametrization of C_j to dimensionless relativeconcentrations C^*_j; k_i and k_{-i} represent the kinetic constant of the forward and the reverse reaction, respectively, and k^*_4, k^*_5 and k^*_7 are parameters involving the ethanol concentration:

$$r_2 = k_2 C_{DHA} \quad (11)$$

$$r_4 = k^*_4\, C_{PA} - k_{-4}\, C_{PAHA} \quad (12)$$

$$r_5 = k^*_5\, C_{PAHA} \quad (13)$$

$$r_6 = k_6 C_{PAHA} \quad (14)$$

$$r_7 = k^*_7\, C_{DHA} - k_{-7}\, C_{GLADA} \quad (15)$$

$$r_8 = k_8\, C_{DHA} - k_{-8}\, C_{OTHERS} \quad (16)$$

$$k^*_4 = C^0_{EtOH}\, k_4 \quad (17)$$

$$k^*_5 = C^0_{EtOH}\, k_5 \quad (18)$$

$$k^*_7 = C^0_{EtOH}\, k_7 \quad (19)$$

The system of differential equations was solved numerically using the methods described in *Section* 2.4. The nine kinetic parameters (k_i and k_{-i}) calculated as described above are presented in Table 3. Results of Table 3 show that the value of k_2 is similar for both catalysts, suggesting that the initial dehydration of DHA is favored on either the Lewis acid sites of SnAl or on the Brønsted acid sites present on the Amberlyst resin. Similar findings were reported by Dapsens et al. [11] and Clippel et al. [14]. Formation of GLADA (step 7) on the other hand, does not proceed on Brønsted sites and occurs with a low rate constant on Lewis acid sites.

The pathway toward PADA from the intermediate compound PA occurs faster on Brønsted acids than on Lewis catalysts, as indicated by the much higher values of k^*_4 (step 4) and k^*_5 (step 5) calculated for the resin. Furthermore, the modeling results show that step 4 is essentially irreversible on the resin. These results can be mechanistically interpreted by considering that the traditional homogeneously catalyzed esterification mechanism on H^+ sites applies on solids with Brønsted acidity [45]. Thus, in Scheme 2 a surface mechanism that interprets the conversion of PA to PAHA and the subsequent esterification of PAHA with ethanol is postulated, previous adaptation from the literature. The conversion of PA to PAHA requires H^+ sites that activate the terminal C=O group of PA. Then, the alcohol molecule attacks the terminal carbonyl of the adsorbed PA species leading to formation of PAHA. The following step involves the activation of PAHA on a proton site, forming a carbocation intermediate that after releasing a H_2O molecule consecutively reacts with another ethanol molecule to give the terminal product, PADA.

Table 3
Kinetic and statistical parameters from modeling of typical Lewis and Brønsted acid catalyzed conversion of DHA with ethanol.

Parameter ($cm^3\ g^{-1}\ h^{-1}$)	Catalyst	
	SnAl	Amberlyst 35W
k_2	43.20 ± 3.19	87.50 ± 5.30
$k_4{}^*$	1160.00 ± 568.00	7220.00 ± 5590.00
$k_5{}^*$	45.40 ± 27.10	275.00 ± 45.90
k_6	200.00 ± 109.00	24.50 ± 6.33
$k_7{}^*$	17.90 ± 3.05	0.00 ± 0.00
k_8	16.40 ± 4.33	31.90 ± 10.80
k_{-4}	8650.00 ± 441.00	0.00 ± 0.00
k_{-7}	6.79 ± 4.26	0.00 ± 0.00
k_{-8}	25.60 ± 11.60	90.30 ± 42.80
R^2	0.98410	0.99332
SSE	0.07425	0.05569
MSC	3.10374	5.11438

Reaction conditions: T = 353 K; P = 250 kPa; DHA/ethanol (molar) = 0.023, W_{cat}/W_{DHA} = 43 wt.%.

The pathway toward EL via PAHA isomerization (step 6 in Scheme 1) is clearly more favored on catalysts with Lewis acid properties. In effect, k_6 was almost 10 times higher on SnAl than on the Amberlyst resin. These results are in line with the catalytic experiments on SnAl (Fig. 2B and Table 2), since EL is obtained with high yields on Lewis acid sites. The EL synthesis occurs mainly by activation and intramolecular rearrangement of PAHA (step 6 in Scheme 1) via a Meerwein-Ponndorf-Verley-Oppenauer (MPVO) mechanism [19]. To a lesser extent, EL could be obtained by direct nucleophilic addition of ethanol to PA, followed by an intramolecular Cannizzaro reaction (step 3 in Scheme 1), as was previously reported using liquid [44] and solid catalysts with Lewis acid properties [8]. However, as explained above, the best modeling results were obtained considering $k_3 = 0$ and therefore, the contribution of this mechanism was ruled out.

Based on our results a surface mechanism to interpret the conversion of PAHA toward EL on the SnAl catalyst is presented in Scheme 3. The participation of an anionic intermediate interacting with surface tin species and that unlikely on other Lewis acids such as Zn-containing catalysts, is postulated. This intermediate, formed by bidentate coordination of PAHA on a Sn atom, undergoes an intramolecular rearrangement with a 1,2-hydride shift to give rise to EL.

The kinetics results of Table 3 were summarized in Scheme 4 where the most favored reaction pathways during DHA conversion on Lewis (Scheme 4A) and Brønsted (Scheme 4B) acid catalysts are depicted. In Scheme 4, the main terminal products obtained are highlighted and the thickness of the arrow lines indicates the relative importance of the reaction steps on each catalyst.

Using these kinetic parameters, the DHA conversion and product yield values predicted by the model were calculated as a function of time. They are shown in Fig. 2 as solid lines. A good visual agreement between experimental (points) and calculated (lines) data was obtained. The parity plot of Fig. 3 involving all the experimental $\left(C^*_{jobs}\right)$ and calculated $\left(C^*_{jcalc}\right)$ relative concentrations of reactant and products for SnAl and Amberlyst 35W gave a statistical confirmation of the model goodness of fit ($R^2 = 0.9723$). Thus, the proposed model gives a suitable description of the DHA conversion reactions on both, Lewis and Brønsted acid solids.

Please cite this article in press as: E.A. Pighin, et al., Kinetic and mechanistic study of triose sugar conversion on Lewis and Brønsted acid solids, Mol. Catal. (2017), http://dx.doi.org/10.1016/j.mcat.2017.11.026

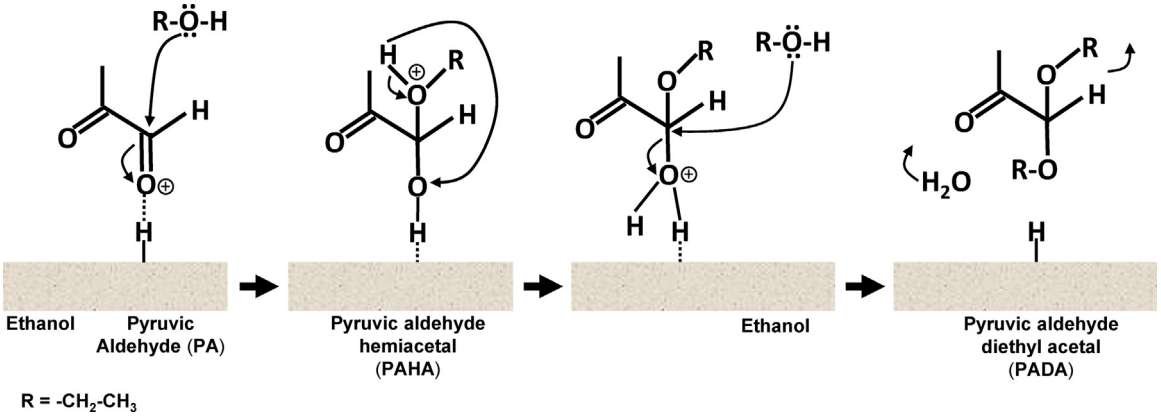

Scheme 2. Postulated surface pathway for conversion of pyruvic aldehyde into pyruvic aldehyde diethyl acetal on Brønsted acid solids.

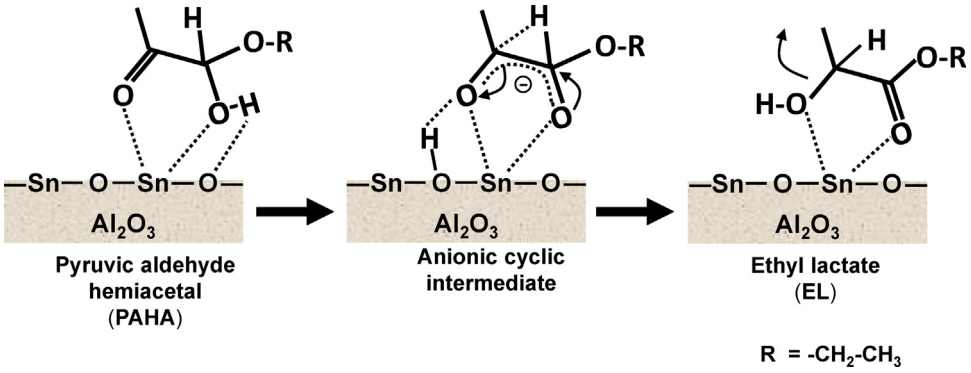

Scheme 3. Postulated surface pathway for synthesis of ethyl lactate on SnAl from pyruvic aldehyde hemiacetal via MPVO mechanism. Adapted from ref. [25].

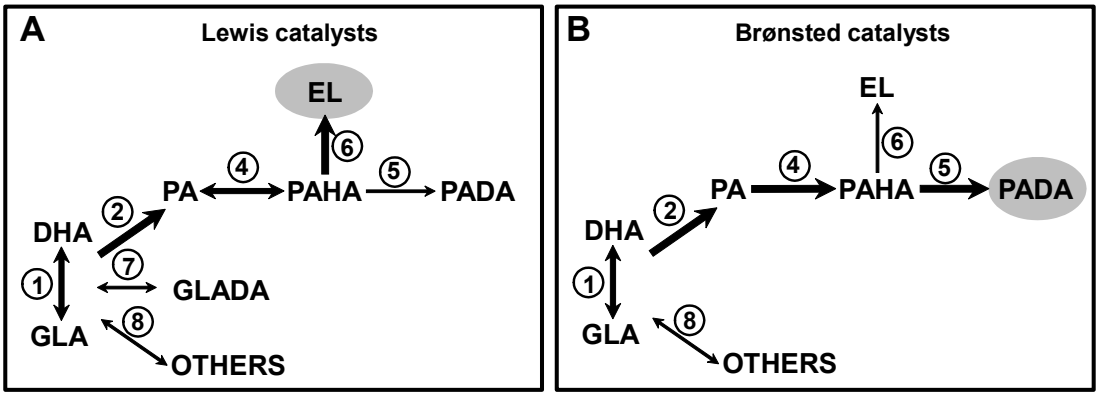

Scheme 4. Simplified reaction pathways for triose conversion from kinetic modeling results on SnAl catalyst (A) and Amberlyst resin (B).

4. Conclusions

The liquid-phase conversion of triose sugars is efficiently promoted both on Brønsted and Lewis solid acid catalysts. The reaction proceeds through a complex reaction network comprising a sequence of consecutive and parallel reaction steps with formation of ethyl lactate and pyruvic aldehyde diethyl acetal as final products. The cesium salt of tungstophosphoric acid and a commercial Amberlyst resin were investigated as Brønsted acid solids whereas alumina-supported tin and zinc oxides were tested as Lewis acid catalysts. The catalytic activity of these materials depends on the chemical nature (Brønsted or Lewis) of the acid sites, but this is not the only factor affecting it. Although Sn and Zn oxides are both Lewis acids, the acid properties, as well as the distinct coordination with reaction intermediates, make the former more active. Brønsted acid solids favor the synthesis of pyruvic aldehyde diethyl acetal, whereas ethyl lactate is the main product on Lewis acid solids.

The kinetics of dihydroxyacetone conversion on Lewis and Brønsted acid solids can be well described by a pseudohomogeneous mechanism and first order rate expressions. Brønsted and Lewis sites promote the initial triose dehydration toward the pyruvic aldehyde intermediate with similar rates. The values of the kinetic rate constants for the following reaction steps confirm that on Brønsted solids the route toward pyruvic aldehyde diethyl acetal occurs at high rates. On Lewis solids, the synthesis of ethyl lactate via isomerization of the pyruvic aldehyde hemiacetal intermediate predominates. Different reaction mechanisms occur on Brønsted and Lewis catalysts. On Brønsted solids, the traditional esterification mechanism on surface H^+ sites takes place, transforming triose

Please cite this article in press as: E.A. Pighin, et al., Kinetic and mechanistic study of triose sugar conversion on Lewis and Brønsted acid solids, Mol. Catal. (2017), http://dx.doi.org/10.1016/j.mcat.2017.11.026

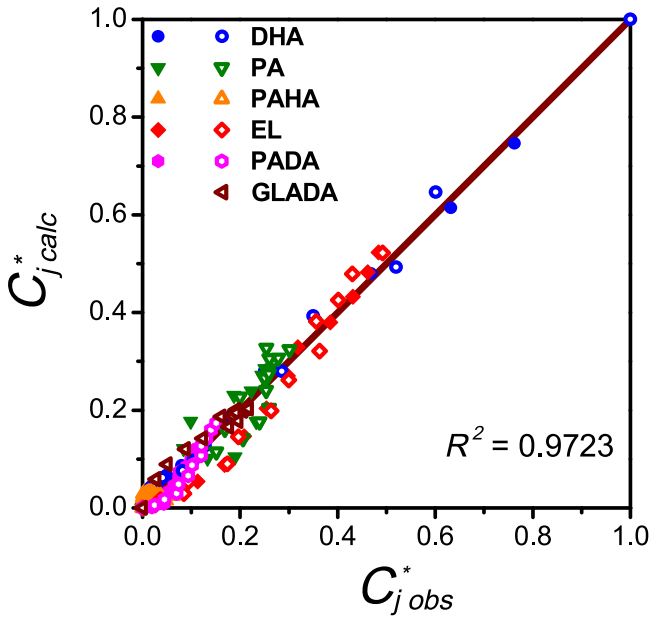

Fig. 3. Parity plot for experimental data and model predictions (closed symbols: Amberlyst 35W resin; open symbols: SnAl catalyst).

sugars into pyruvic aldehyde hemiacetal and diethyl acetal with the release of H_2O molecules. On the other hand, on catalysts with Lewis acid properties, the pyruvic aldehyde hemiacetal intermediate coordinates with metal cations (particularly Sn^{4+}) forming a cyclic intermediate that undergoes an intramolecular rearrangement with a 1,2-hydride shift, yielding ethyl lactate.

Acknowledgements

Authors thank the Agencia Nacional de Promoción Científica y Tecnológica (ANPCyT), Argentina (Grant PICT 1857/15), CONICET, Argentina (grant PIP 11220090100203/10) and Universidad Nacional del Litoral, Santa Fe, Argentina (grant CAID PI 007-040/05) for financial support of this work.

Appendix A. Supplementary data

Supplementary data associated with this article can be found, in the online version, at http://dx.doi.org/10.1016/j.mcat.2017.11.026.

References

[1] A. Corma, S. Iborra, A. Velty, Chem. Rev. 107 (2007) 2411–2502.
[2] E.L. Kunkes, D.A. Simonetti, R.M. West, J.C. Serrano-Ruiz, C.A. Gärtner, J.A. Dumesic, Science 322 (2008) 417.
[3] G.W. Huber, S. Iborra, A. Corma, Chem. Rev. 106 (2006) 4044–4098.
[4] K.T. Narayana, US Patent 6342626, 2002.
[5] T.N.B. Kaimal, P. Vijayalakshmi, B. Ramalinga, A. A. Laxmi, US Patent N° 6342626, 2002.
[6] D.I. Weisblad and B.J. Magerlein, US 2631149 (1953), to Kalamazoo Corporation.
[7] M.S. Jensen, M. Palucki, N.R. Rivera, K. Wells, Y. Xiao, Y. Wang, Ch. Yang, N. Yasuda, WO 2202191 (2000), to Merck & Co., Inc.
[8] P.P. Pescarmona, K.P.F. Janssen, C. Delaet, C. Stroobants, K. Houthoofd, A. Philippaerts, C. De Jonghe, J.S. Paul, P.A. Jacobs, B.F. Sels, Green Chem. 12 (2010) 1083–1089.
[9] R.M. West, M.S. Holm, S. Saravanamurugan, J. Xiong, Z. Beversdorf, E. Taarning, C.H. Christensen, J. Catal. 269 (2010) 122–130.
[10] K.P.F. Janssen, J.S. Paul, B.F. Sels, P.A. Jacobs, Stud. Surf. Sci. Catal. 170 (2) (2007) 1222–1227.
[11] P.Y. Dapsens, B.T. Kusema, C. Mondelli, J. Pérez-Ramírez, J. Molec. Catal. A: Chem. 388–389 (2014) 141–147.
[12] A.M. Mylin, S.I. Levytska, M.E. Sharanda, V.V. Brei, Catal. Comm. 47 (2014) 36–39.
[13] L. Li, C. Stroobants, K. Lin, P.A. Jacobs, B.F. Sels, P.P. Pescarmona, Green Chem. 13 (2011) 1175–1181.
[14] F. de Clippel, M. Dusselier, R. Van Rompaey, P. Vanelderen, J. Dijkmans, E. Makshina, L. Giebeler, S. Oswald, G.V. Baron, J.F.M. Denayer, P.P. Pescarmona, P.A. Jacobs, B.F. Sels, J. Am. Chem. Soc. 134 (2012) 10089–10101.
[15] C.M. Osmundsen, M.S. Holm, S. Dahl, E. Taarning, Proc. R. Soc. A (2012) 1–17.
[16] N. Godard, A. Vivian, L. Fusaro, L. Cannavicci, C. Aprile, D.P. Debecker, Chem Cat Chem (2017), http://dx.doi.org/10.1002/cctc.201601637, in press.
[17] J. Wang, Y. Masui, M. Onaka, Appl. Catal. B: Environ. 107 (2011) 135–139.
[18] H.J. Cho, P. Dornath, W. Fan, ACS Catal. 4 (2014) 2029–2037.
[19] E. Taarning, S. Saravanamurugan, M. Spangberg Holm, J. Xiong, R.M. West, C.H. Christensen, Chem. Sus. Chem. 2 (2009) 625–627.
[20] J. Dijkmans, M. Dusselier, D. Gabriels, K. Houthoofd, P.C.M.M. Magusin, S. Huang, Y. Pontikes, M. Trekels, A. Vantomme, L. Giebeler, S. Oswald, B.F. Sels, ACS Catal. 5 (2015) 928–940.
[21] C. Hammond, S. Conrad, I. Hermans, Angew. Chem. Int. Ed. 51 (2012) 11736–11739.
[22] S. Tolborg, A. Katerinopoulou, D.D. Falcone, I. Sádaba, C.M. Osmundsen, R.J. Davis, E. Taarning, P. Fristrup, M.S. Holm, J. Mater. Chem. A 2 (2014) 20252–20262.
[23] W.N.P. van der Graaff, G. Li, B. Mezari, E.A. Pidko, E.J.M. Hensen, ChemCatChem 7 (7) (2015) 1152–1160.
[24] E. Pighin, V.K. Díez, J.I. Di Cosimo, Appl. Catal. A: General 517 (2016) 151–160.
[25] E. Pighin, V.K. Díez, J.I. Di Cosimo, Catal. Today 289 (2017) 29–37.
[26] O. Acarbas, E. Suvacı, A. Dogan, Ceram. Int. 33 (2007) 537–542.
[27] D.E. Mears, Ind. Eng. Chem. Proc. Des. Dev. 10 (4) (1971) 438–447.
[28] P.B. Weisz, C.D. Prater, Adv. Catal. 6 (1954) 143–196.
[29] R.E. Walpole, R.H. Myers, S.L. Myers, K.E. Ye, Probability & Statistics for Engineers & Scientists, 8th Ed., Pearson Prentice Hall, 2007.
[30] S. Armenise, E. García-Bordeje, J.L. Valverde, E. Romeo, A. Monzón, Phys. Chem. Chem. Phys. 15 (2013) 12104–12117.
[31] I. Kozhevnikov, Chem. Rev. 98 (1998) 171.
[32] S. Tatematsu, T. Hibi, T. Okuhara, M. Misono, Chem. Lett. (1984) 865–868.
[33] Y. Izumi, K. Hisano, T. Hida, Appl. Catal. A: Gral. 181 (1999) 277–282.
[34] S. Soled, S. Miseo, G. McVicker, W.E. Gates, A. Gutierrez, J. Paes, Chem. Eng. J. 64 (1996) 247.
[35] B. Bachiller-Baeza, J.A. Anderson, J. Catal. 228 (2004) 225–233.
[36] S. Toppi, C. Thomas, C. Sayag, D. Brodzki, K. Fajerwerg, F. Le Peltier, C. Travers, G. Djéga-Mariadassou, J. Catal. 230 (2005) 255–268.
[37] V.K. Díez, C.R. Apesteguía, J.I. Di Cosimo, Catal. Lett. 123 (2008) 213–219.
[38] K. Tanabe, M. Misono, Y. Ono, H. Hattori, New solid acids and bases their catalytic properties, in: K. Tanabe, M. Misono, Y. Ono, H. Hattori (Eds.), Stud. Surf. Sci. and Catal., vol. 51, 1989 (p. 82 Elsevier ISBN: 978-0-444-98800-3).
[39] J. Penzien, A. Abraham, J.A. van Bokhoven, A. Jentys, T.E. Muller, C. Sievers, J.A. Lercher, J. Phys. Chem. B 108 (2004) 4116–4126.
[40] T. Takewaki, L.W. Beck, M.E. Davis, J. Phys. Chem. B 103 (1999) 2674–2679.
[41] M. Orazov, M. Deimund, M.E. Davis 24th., North American Catalysis Society Meeting Proceeding, 14–19th, June 2015, Pittsburgh (USA), O-W-A-15, 2015.
[42] R.T. Sanderson, Chemical Bonds and Bond Energy, 2nd Ed., Academic Press, New York, 1976.
[43] V.K. Díez, P.A. Torresi, P.J. Luggren, C.A. Ferretti, J.I. Di Cosimo, Catal. Today 213 (2013) 18–24.
[44] Y. Hayashi, Y. Sasaki, Chem. Commun. (2005) 2716–2718.
[45] R.T. Morrison, R.N. Boyd, Organic Chemistry, 6th Ed., Prentice-Hall, New York, 1959, pp. 680.